Colloids and Surfaces A: Physicochemical and Engineering Aspects 665 (2023) 131207

Contents lists available at ScienceDirect

Colloids and Surfaces A: Physicochemical and Engineering Aspects

journal homepage: www.elsevier.com/locate/colsurfa

Evaporation dynamics of a sessile milk droplet placed on a hydrophobic surface

Binita Pathak [a,*], John Christy [b]

[a] Department of Mechanical Engineering, Indian Institute of Technology, IIT-BHU Varanasi, Varanasi 221005, India
[b] School of Engineering, the University of Edinburgh, Kings Buildings, Edinburgh EH9 3JL, United Kingdom

HIGHLIGHTS

- Protein-laden milk droplets on hydrophobic substrates depict cavitated structures beyond a critical protein concentration.
- As the initial concentration of protein exceeds a threshold value, buckling instability initiates and leads to cavitated final structures.
- The buckling phenomena is initiated due to imbalance of stresses but is driven by evaporation of solvent in the droplet.

GRAPHICAL ABSTRACT

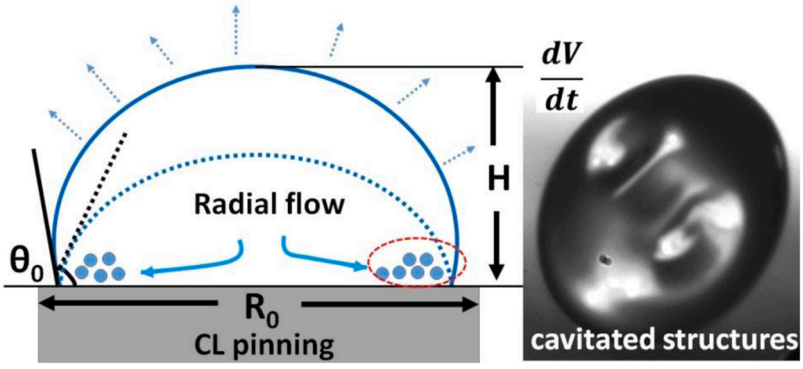

ARTICLE INFO

Keywords:
Droplet dynamics
Hydrophobic surface
Internal flows
Protein
Buckling instability

ABSTRACT

A colloidal droplet is an integral part of spray-drying based applications such as food, pharmaceuticals, drug delivery, etc. The complex physico-chemical dynamics determine the final structures obtained in the process. Therefore, a complete understanding of the different forces involved and the evaluation of the governing parameters is crucial to control the final morphologies as desired. The evaporation-induced dynamics are studied in milk droplets placed on hydrophobic substrates under natural drying condition. Experiments were performed systematically by varying the initial concentration of protein (BSA) in the droplets. The results were analyzed using energy-based models. Capillary forces and inter-particle interaction are found to have dominating effects upon the particle deposition in the evaporating droplets. Furthermore, inclusion of protein beyond a threshold initial concentration leads to buckling instability which produces cavitated structures. Maintenance of hydrophobicity for a sufficient amount of time is an important criterion to initiate the buckling instability. Our study provides physical insights into the dynamics involved in desiccating droplets, including the buckling dynamics. These insights have far-reaching implications in spray-based industries.

* Corresponding author.
E-mail addresses: binita.mec@itbhu.ac.in, binitapathak88@gmail.com (B. Pathak).

https://doi.org/10.1016/j.colsurfa.2023.131207
Received 6 January 2023; Received in revised form 13 February 2023; Accepted 25 February 2023
Available online 1 March 2023

1. Introduction

Drying colloidal droplets are crucial in many pharmaceutical, food and dairy industries [1–4]. The process of drying is complex as it induces internal flow field in the droplet which causes collision and aggregation of particles leading to the formation of final structures [5,6]. The desirable structures are also applicable in the development of sensors, electronics and in drug delivery, among many other applications. The complex dynamics involved in the process of drying have been studied previously using pendant, sessile and levitated droplets [7–13]. For instance, the particles in a sessile colloidal droplet are carried along with the internal flow which gets deposited in the peripheral region, forming a ring. This well-known coffee ring deposit was first investigated by Deegan [14]. After this, Weon and Je employed a simple force balance model to explain the self-pining mechanism due to solute confinement leading to such ring-type deposits in colloidal droplets [15]. They determined the order of magnitude of different forces and found that the capillary force has a dominating effect upon the self-pinning of droplets. The evaporation dynamics involved in a sessile droplet was also studied theoretically by Picknett and Bexon and numerically by Hu and Larson [16,17]. A mathematical model was developed to evaluate the rate of evaporation in such droplets which matches well with the experimental data. Maki and Kumar also simulated the evaporation dynamics of a sessile colloidal droplet [18]. They solved the governing equations to evaluate a gradual variation in particle concentration along the depth of the droplet. The particles undergo agglomeration and form a skin at the surface of the droplet, thereby influencing the final structures. In addition to the evaporation rates, the final morphologies also depend upon the initial composition of the solution. For example, inclusion of ellipsoidal shaped particles eliminates the ring-shaped pattern and a more uniform final deposition is obtained in drying sessile droplets [19]. The effect of other parameters such as heating and particle sizes were also studied using sessile droplets [20]. A regime map was determined by Patil et. al for sessile droplets based on the types of deposits formed due to self-sorting of particles according to size as well as the effect of heat [20]. The transition of patterns from ring to film deposits was theoretically modeled by Kaplan and Mahadevan [6]. The transition was defined based on the initial concentration of the particles and an inverse capillary number which represents the ratio of viscous to capillary forces. The properties of the substrate also play a crucial role in determining the patterns of the final deposition [21]. The substrate roughness manipulates the contact line dynamics which controls the droplet dynamics and influences the final deposition patterns. Another important governing parameter is the hydrophobicity of the substrate. Droplets placed on a hydrophobic substrate usually shows a buckling instability leading to a cavity formation in the final structure [22]. Therefore, it can be seen that the final morphologies is a resultant of many factors and can thus be manipulated by regulating these governing parameters. However, the entire droplet dynamics is a complex interplay of different processes and a detailed understanding of these processes is crucial.

In the current study, we chose milk droplets as the base colloidal suspension and studied the evaporation dynamics by varying the initial concentration of protein in the droplets. We have chosen BSA as the added protein as it is an important milk protein. Drying of protein droplets is fundamental in spray drying processes involved in many industries [23]. Spray drying leads to complex physicochemical changes in the droplets which are difficult to predict [24]. Therefore, a single protein droplet is an excellent platform to understand the drying behavior [25]. We have investigated the drying of a single droplet placed on a hydrophobic substrate to provide physical insights into the dynamics of such droplets. Although, a substrate might induce additional complexities, the evaporation induced dynamics remain unaltered. Therefore, the results of sessile droplet configuration can provide fundamental insights into the drying process of a spray system. Both the evaporation and particle dynamics play a crucial role in the development of the final structures. It was also observed that a threshold initial protein concentration is required to initiate buckling instability in the droplets which leads to cavitated final structures. All the experiments in the current study were performed under natural drying condition to avoid additional complexity due to heat.

2. Material and methods

2.1. Solution preparation

Bovine Serum Albumin (BSA) was purchased from Sigma Aldrich, UK and was used as is by dissolving in skimmed milk. The skimmed milk without adding BSA was used as the base case. The experiments were performed by varying the initial concentration of BSA (3 %−7 % by wt.) to understand the effect of protein concentration upon the droplet dynamics. The fluid properties were estimated by using the mixing law (by considering milk droplet as the base case, i.e., 0 wt% BSA) (Table 1).

2.2. Experiments

The experiments were performed using droplets of an initial volume of 3 μl which were placed on hydrophobic perfluorodecyltrichlorosilane (FDTS) surfaces. The surfaces were prepared using silicon base with micro pillars systematically arranged on it and then coated with FDTS through vapor deposition. The fabrication was done using photolithography and deep reactive ion etching (DRIE) techniques [26]. The details of surface preparation are given elsewhere [27].

The droplets were dispensed using an automatic dispenser in a drop shape analyser [KRUSS, DSA100] and left to dry at the room temperature of (24–25 °C) and relative humidity of 32–37 %. The initial contact angles of the droplets were around 95–100°. The droplet dynamics were monitored using shadowgraphy (back-illumination) technique and a digital camera [MAKO G, Allied Vision Technologies]. The images were captured at 1 fps and processed using ImageJ software. The final deposited structures were studied under an optical microscope. The schematic of the experimental set-up is shown in Fig. 1. The experiments were performed 5 times for each case for repeatability.

3. Results and discussion

The capillary number for the droplets used in the current study was around 0.2 and hence the effect of gravity was neglected in the study. The entire lifetime of the drying droplets can be divided into two stages (shown in Fig. 2). The first stage is the pure evaporation stage, when the droplets undergo constant contact radius (CCR) mode of evaporation. The protein molecules strongly adhere to the substrate which pins the contact line throughout the droplet lifetime. The drying is thus characterized by a reduction in the droplet contact angle (θ) and its height (H) (Fig. 3). Both the height and the contact angle reduce continuously upto time t_0 (Fig. 2(b)). As the solvent evaporates, a capillary flow is generated within the droplet which carries the solute particles and deposits in the peripheral region. The accumulation of the solute particles leads to the development of a thick deposit (d_{t0}) at the end of the CCR mode (t_0). The height (H) is approximately 50 % of the initial height (H_0) at this point of time. The deposition of a thick ring at the periphery fixes the contact angle at $\theta_{t0}\left(\sim 55^0 to 60^0\right)$ in time t_0 and θ_{t0}do not change any further throughout the process of drying. This $\theta_{t0}$is about 60 % of the initial contact angle (θ_0). A pseudo contact angle θ' can then be identified to be formed by the liquid-air interface of the droplet on the

Table 1
Properties of the fluids used in the experiments.

Concentration (wt%)	Density (kg/m^3)	Viscosity (Ns/m^2)
0	1035	0.0015
3	1038	0.0016
7	1041	0.0018

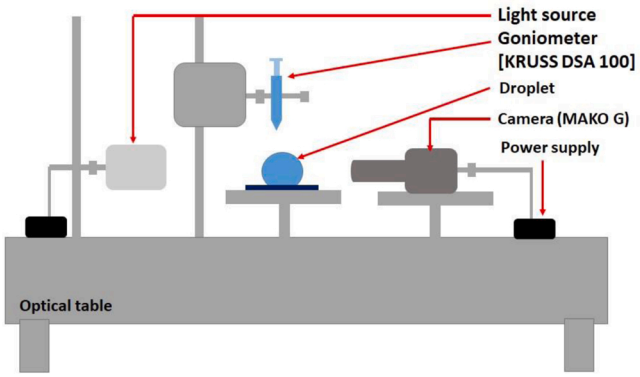

Fig. 1. Schematic of the experimental set-up.

peripheral deposit (of thickness d_{t0}) (Fig. 2(c)). The evaporation of solvent continues which causes a reduction in θ' and H which continues till the end of the drying process (Mode 2 in Fig. 3(b)). This can be referred to as the second stage of drying. It is to be noted that the dramatic change in the trend of the graph of θ (at t_0) is due to the consideration of the pseudo contact angle θ' after t_0 and not the actual contact angle θ which remains constant after t_0. The height (H) continues to decrease throughout the lifetime of the droplet down to the final deposit height "d_{f0}" (130–400 μm) (Fig. 2(d)). The mode 2 is followed by buckling of the droplets (inset: Fig. 2(d)). Buckling is a structural instability which is initiated at the weak points on the droplet surface (beyond a critical BSA concentration), leading to a cavity formation on the surface. The final deposit is shown in Fig. 2(e) [inset: top view] which depicts the buckled final structures. The different stages are explained in the following sections.

3.1. Evaporation dynamics of the droplets

The droplet placed on the substrate can be considered as a spherical cap of initial radius R_0, height H_0 (at the center) and contact angle θ_0. As the solvent evaporates, both the H and θ change (as the contact radius is fixed at R_0) and a new equilibrium state is attained by the system. The new equilibrium state of the droplet (at any time instant) requires minimization of the total energy of the droplet (E). The temporal evolution of the system is thus evaluated by minimizing the total energy of the droplet which is given as:

$$\frac{dE}{dt} = 0 \tag{1}$$

The rate of change of total energy of the droplet (E) is given as:

$$\frac{dE}{dt} = \dot{E}_f + \dot{E}_{visc} \tag{2}$$

(Here, $\dot{E}_f$ and $\dot{E}_{visc}$ are the rate of change of free energy of the droplet and the viscous dissipation rate respectively).

The free energy of the droplet can be approximated as:

$$E_f = \sigma\,\pi\left(R^2 + H^2\right) \tag{3}$$

(Here, R is the contact radius which is equivalent to R_0 throughout and H is the height at the center of the droplet. σ is the coefficient of surface tension of the droplet).

The viscous dissipation rate for the droplet is given as:

$$\dot{E}_{visc} = \int_0^R \mu \frac{u^2}{\delta} 2\pi r dr \tag{4}$$

(Here, u is the internal flow velocity. The velocity is considered to be uniform across various protein concentrations and $\delta \sim \sqrt{\frac{r\mu}{\rho u}}$ is the boundary layer thickness. μ and ρ are the viscosity and density of the solution respectively).

The temporal variation of the droplet height (H) is thus evaluated by using Eqs. (1)–(4) as:

$$H\frac{dH}{dt} = -\frac{2}{3}\frac{R^{3/2}u^{5/2}\sqrt{\mu\rho}}{\sigma} \tag{5}$$

Eq. (5) is non-dimensionalized using the initial droplet height H_0 as the characteristic length scale which gives:

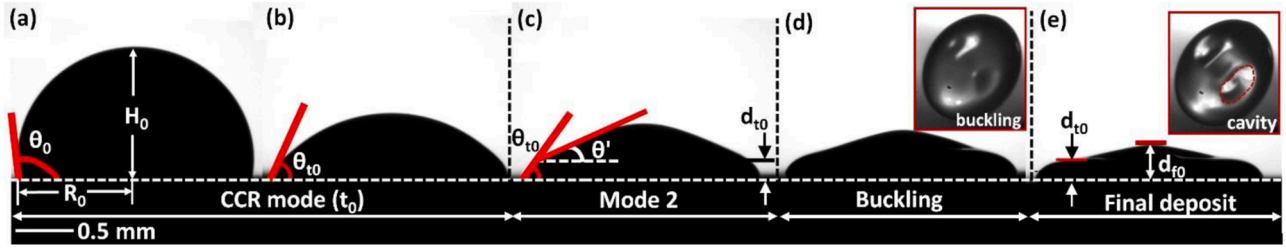

Fig. 2. Evaporation dynamics of the droplets (shown only for 7 wt% BSA droplets; $H_0 \sim 1$ mm, $\theta_0 \sim 92^0 - 97^0$) [inset: top views of (d) buckling initiation and (e) the final cavitated deposit].

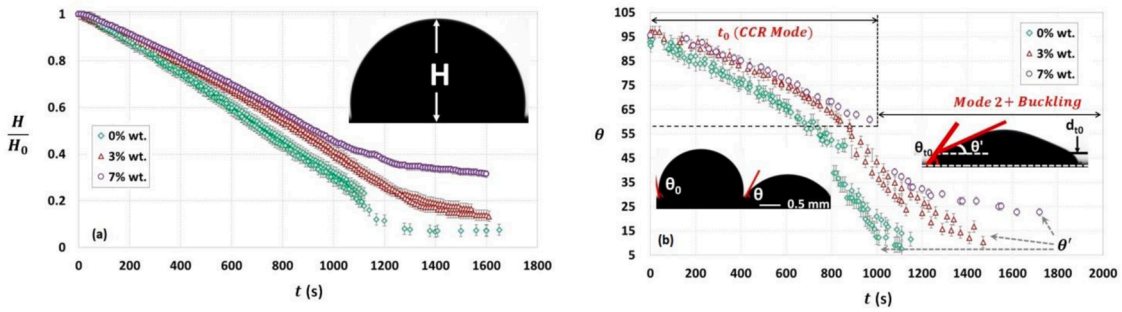

Fig. 3. Temporal variation of (a) droplet height (non-dimensionalized with the initial value H_0) and (b) droplet contact angle (θ) [θ remains constant after t_0; the data is then plotted for θ' after t_0 (t_0 is shown only for one concentration for clarity but the trends are similar across all the cases)] (color online).

$$\overline{H}\frac{d\overline{H}}{d\bar{t}} = -\frac{2}{3} \quad (6)$$

Here, $\overline{H} = \frac{H}{H_0}$ and $\bar{t} = \frac{t}{t_c}$. The characteristic timescale is thus derived as: $t_c \sim \frac{\sigma {H_0}^2}{R^{3/2}u^{5/2}\sqrt{\mu\rho}}$ by using Eq. (5).

The non-dimensionalized Eq. (6) is then integrated to determine the temporal variation of the height $\overline{H}$ as:

$$\overline{H}^2 = 1 - \frac{2}{3}\bar{t} \quad (7)$$

The appropriateness of the timescale (t_c) evaluated by non-dimensionalization of Eq. (5) is validated by the collapse of all the $\overline{H}^2 = \left(\frac{H}{H_0}\right)^2$ data plotted against $\bar{t} = \frac{t}{t_c}$ across the different solutions used in this study (Fig. 4). The presence of particles will not influence the droplet dynamics initially due to dilute concentration. However, gradual agglomeration of the particles will affect the flow and the dynamics of the droplet will deviate from the model. The deviation of experimental data from the model is observed towards the end of the droplet lifetime in Fig. 4.

Although the fluid motion and drop shape (droplet dynamics) are governed by all the forces acting on the drop, the internal behavior of particulate and precipitating components play a significant role. The effect of particle dynamics is evident in the rate of decrease of droplet volume (Fig. 5). The initial rate of evaporation is similar in all the cases due to similar surface area of all the droplets (0–7 wt% BSA). The evaporation generated internal flow field ($\sim$ O (10^{-7}) m/s) causes deposition of particles in the peripheral region. The deposit reduces the surface area available for further evaporation ($\sim$15 % reduction for 0 wt % BSA and $\sim$28 % for 7 wt% BSA). The reduction in surface area is revealed as a reduction in the rate of volumetric decay in the protein laden droplets as compared to the base case (pure milk droplets) (Fig. 5). The decrease in evaporation rate is more prominent at higher concentration of BSA (7 wt%) towards the end as more particles are deposited and causes a significant reduction in the surface area available for evaporation of the droplets. The surface area reduces continuously upto A which is approximately 50–55 % of the initial surface area (A_0) of the droplet. Henceforth, the area does not change any further.

3.2. Particle dynamics

Different forces act upon the particles within the droplet due to both inter particle interactions and hydrodynamic interactions. The major forces acting upon the particles include the capillary force which is given as: $F_{cap} = 2\pi r_p \sigma \cos^2\theta$ (where, r_p is the particle radius $\sim$ 3 nm and $\theta$is the contact angle formed at the liquid-particle interface. σ is the coefficient of surface tension of the droplet). The capillary forces lead to the

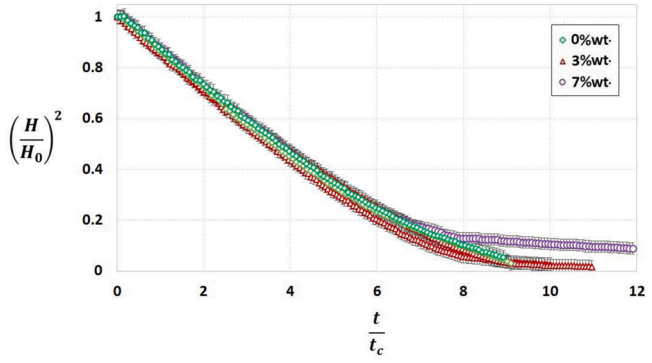

Fig. 4. Temporal variation of the droplet height (H) (non-dimensionalized with the initial height (H_0). Time (t) is non-dimensionalized with $t_c \sim c_1 \frac{\sigma {H_0}^2}{R^{3/2}u^{5/2}\sqrt{\mu\rho}}$($c_1$ is some constant). (color online).

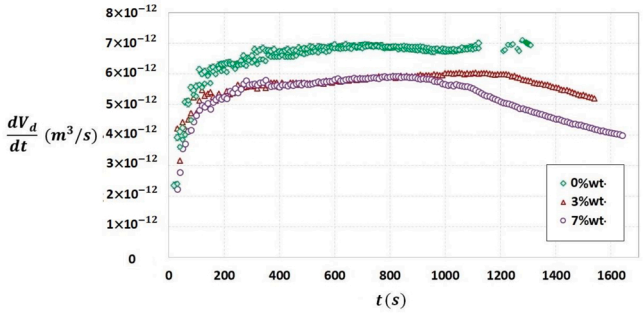

Fig. 5. Temporal variation of the volumetric decay rate of the droplets (V_d is the droplet volume). (color online).

deposition of particles in the peripheral region [15]. The evaporation of the solvent induces a flow within the droplet. This internal fluid flow exerts a drag force upon the particles which is given as: $F_{drag} = 6\pi r_p \mu v_i$ (where, v_i is the internal flow velocity). The drag force $\left(F_{drag} \sim O(10^{-17})\ N\right)$is smaller than the capillary forces $\left(F_{cap} \sim O(10^{-11})N\right)$ by several orders of magnitude and hence will have a negligible influence upon the particle dynamics. The interactions between particle-particle and particle-substrate within the droplet exert DLVO forces which consist of van der Waals forces $F_{van} = \left(\frac{2A}{3}\right)\frac{{r_p}^3}{D^2(D+2r_p)^2} + \left(\frac{A}{12}\right)\frac{r_p}{D^2}$ and electrostatic forces $F_{elec} = \kappa Z r_p e^{-\kappa D}$, where, A is Hamaker constant $\left(\sim 5\times10^{-20}\ J\right)$, D is the separation distance between the particles $\left(\sim O\left(10^{-9}\right) m\right)$, κ^{-1} is Debye length ($\sim O(10^{-9})$ m), $Z = 63\pi\varepsilon\varepsilon_0\left(\frac{k_B T}{e}\right)^2 \tanh\left(\frac{ze\Psi_0}{4k_B T}\right)\tanh\left(\frac{ze\Psi_s}{4k_B T}\right)$; ε and ε_0 are the dielectric constant and the permittivity of free space respectively, e is electron charge, z is surface charge, k_B is the Boltzmann constant and T is the temperature. Ψ_0 and Ψ_s are the zeta potential of the particles and the substrate respectively [28].

The DLVO forces ($F_{DLVO} = F_{van} + F_{elec}$) are of the similar orders as the capillary forces (F_{cap}) initially (when the contact angle is $\theta > 90^0$). Therefore, a uniform deposition is formed on the substrate due to particle adhesion (due to DLVO forces) alongside the peripheral particle deposition due to the capillary flow. However, it can be perceived from the rapid increase in capillary forces that it ($F_{cap} \sim 10^{-9}$ N) soon dominates the dynamics of particles within the droplet (Fig. 6). The DLVO forces increases gradually throughout the droplet lifetime due to an increase in particle interactions with the loss of solvent caused by evaporation (Fig. 6). The forces are marginally higher at higher particle concentration ($F_{DLVO,7\%wt.} > F_{DLVO,3\%wt.}$) due to more interaction among particles at higher concentration within the similar droplet volume. This leads to a thicker deposition at the periphery at higher particle concentration ($d_{f0} \sim 400$ μm and ~ 200 μm at 7 wt% and 3 wt% respectively) at the end of the droplet lifetime.

The experimental set-up is used in the current work to investigate the dynamics in the macroscopic level (droplet-system parameters) and is not suitable for investigation at the scale of individual particles. The inter-particle dynamics require rigorous microscopic investigation for the exact estimation of all the forces. However, the qualitative analysis of the microscopic (particle-level) forces undertaken in this work demonstrates the influence of particle dynamics upon the final deposition.

3.3. Buckling dynamics of the droplets

The loss of solvent causes a concentration gradient throughout the droplet with the highest concentration of solutes at the droplet surface. The protein particles undergo sol-gel transition which leads to the development of a thin skin at the droplet surface. This type of skin formation has been observed during drying of many colloidal solutions [10, 13,29]. The skin behaves like an elastic membrane under stress (P_b) due

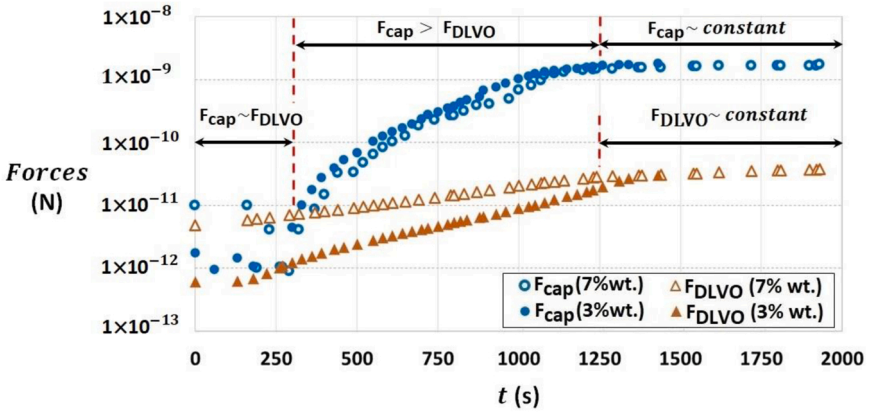

Fig. 6. Temporal variation of the capillary forces (F_{cap}) and DLVO forces (F_{DLVO}) [data is shown for 3 wt% (closed symbols) and 7 wt% of BSA (open symbols) respectively].

to continuous decrease in the droplet volume caused by the evaporation. As the stress (P_b) exceeds the critical value (P_{crit}), the membrane undergoes buckling instability. Buckling is initiated at the weak points with minimum Gaussian curvature on the droplet surface. It initiates as a deformation (dent) and proceeds into negative curvatures (i.e, cavity) to attain a stable equilibrium state (insets: Fig. 2(d, e)). The elastic membrane resists the deformation on account of its elastic energy which is of the order of $E \sim O\left(\frac{Yh_s^{5/2}H_b^{3/2}}{r_b}\right)$ [here, Y is Young's modulus of the membrane, h_s is the membrane thickness, H_b is the buckled cavity depth, and r_b is the radius of the buckling cavity.]. The cavities are created when the membrane can no longer resist the deformation. Multiple cavities indicate multiple weak points on the surface of the membrane (Fig. 2e). The energy equation governing the buckling dynamics is then given as:

$$\frac{dQ}{dt} = \frac{dW}{dt} + \frac{dE}{dt} + \frac{d(m_d c_v T)}{dt} + \rho_w h_{fg} \frac{dV_{cav}}{dt} \tag{8}$$

Here, Q is the external heat supplied. Under natural drying condition, $Q = 0$. The work done due to stress ($W \sim P_b V_{cav}$) and elastic energy (E) are of similar orders (O (10^{-6}) J) which are comparatively lower than the other terms on the RHS of Eq. (8). Therefore, Eq. (8) gives a scaling approximation as:

$$\frac{dV_{cav}}{dt} \sim \frac{c_v T}{\rho_w h_{fg}} \frac{d(\rho_d V_d)}{dt} \tag{9}$$

The cavity volume (V_{cav}) plotted using the approximation Eq. (9) shows a reasonable match with the experimental values (Fig. 7(a)) and thus justifies the scaling approximation stating that the buckling $\left(\frac{dV_{cav}}{dt}\right)$ is driven by evaporation of liquid trapped inside the droplet.

Furthermore, it has been observed that the buckling is initiated only above a threshold concentration of BSA ($\varnothing_{init} > 5$ % wt.) [the experiments were performed for various BSA concentrations, upto 9 wt% to confirm the threshold value]. The change in shape of the droplet due to evaporation has a direct influence upon the buckling dynamics. Buckling is a structural instability which requires a dome-shaped structure as a pre-requisite. All the droplets placed on FDTS substrates are hydrophobic initially (i.e, contact angle, $\theta > 90^0$) which leads to a dome-type shape of the droplet (Fig. 2(a)). However, the hydrophobicity is lost due to continuous evaporation of the solvent and decrease in the droplet volume. A timescale is defined as $t_{\theta<90}$ which indicates the time required by the droplet to lose its hydrophobicity (i.e, $\theta < 90^0$). This timescale should be sufficiently large to allow the sol-gel transition of the proteins and the initiation of the buckling phenomena. It has been observed that the buckling is initiated almost immediately after the mode 1 is completed at time t_0. Therefore, a transition criterion is determined as the ratio $\frac{t_{\theta<90}}{t_0}$ such that a clear demarcation of ~ 0.15 is obtained to distinguish the buckling and no-buckling regimes above an initial BSA concentration of 5 wt% (Fig. 7(b)). Furthermore, a plot of the ratio $\frac{H_b}{R_b}$ (where, H_b and R_b are the height and the contact radius of the droplet respectively) at time t_0 shows a gradual increase with an increase in the initial concentration of BSA in the droplets. Accordingly, it can be observed that a higher value of $\frac{H_b}{R_b}$ (> 0.5) is required for the initiation of buckling. Both the criteria $\left(\frac{t_{\theta<90}}{t_0} \geq 0.15 \text{ and } \frac{H_b}{R_b} \geq 0.5\right)$ indicates that hydrophobicity is an important parameter to initiate the buckling phenomena although once initiated the buckling is driven solely by the evaporation of the solvent in the droplet.

4. Conclusions

In this paper, we have explored the different stages of a desiccating milk-based droplet placed on a hydrophobic substrate. Earlier works

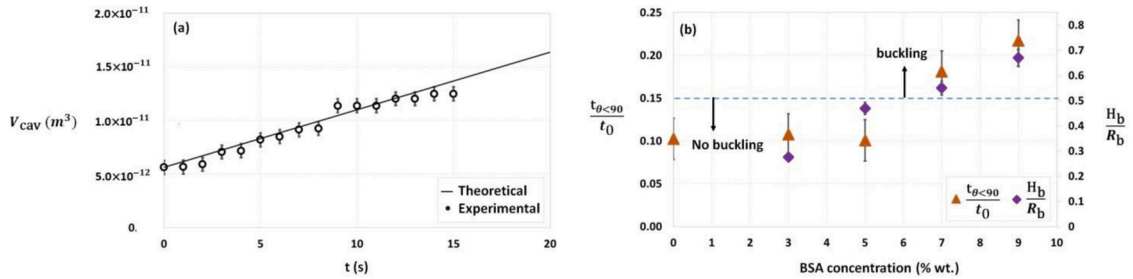

Fig. 7. (a) Temporal variation of cavity volume (shown for droplets of 7 wt% BSA) and (b) Variation of $\frac{t_{\theta<90}}{t_0}$ (primary axis) [$t_{\theta<90}$:time required by the droplet to lose its hydrophobicity which is determined by the contact angle (θ) being less than 90^0; t_0: time required for CCR mode of evaporation (mode 1)]; variation of the ratio of droplet height (H_b) to radius (R_b) at t_0 (secondary axis).

have investigated the deposited patterns formed of different colloidal droplets [30–33] but the overall dynamics involved in the drying process is not yet clear. The particles in a colloidal droplet are driven by internal flows which form a ring-type structure on the substrate [14,15]. However, the patterns are different in protein droplets and are more uniform on the substrate. The plausible reason for this was discussed based on inter-particle interactions and strong affinity of the particles to the substrate. The variation of protein concentration is studied extensively for the first time using milk droplets under natural drying condition. This work explains the evaporation dynamics using an energy-based model which validates the experimental data. The capillary forces and inter-particle interactions are found to be equally dominant initially but the capillary force rapidly rises and causes a thick peripheral deposition on the substrate. Furthermore, a buckling instability is observed to be initiated beyond a threshold concentration of protein in the droplets. The suppression of buckling below the threshold concentration of protein is attributed to the loss of hydrophobicity before the onset of the sol-gel transition of the protein layer at the surface of the droplet. The scaling analysis of the governing energy equation shows that although the buckling is initiated due to imbalance of stresses, it is driven by the evaporation of solvent in the droplet. The physical insights obtained in this work can be extended to high throughput processes like sprays applicable in pharmaceutical, drugs and food-based industries.

As a future scope, further investigation can be carried out using different substrates to understand if the dynamics and the governing forces alter. Inclusion of multiple proteins will affect the inter-particle interaction which plays a crucial role in producing the final structures. Therefore, further studies regarding the effect of multiple proteins can be carried out using sessile droplets.

CRediT authorship contribution statement

Binita Pathak: Visualization, Data curation, preparation, Writing – original draft. **John Christy:** Conceptualization, Methodology, Supervision.

Declaration of Competing Interest

The authors declare that they have no known competing financial interests or personal relationships that could have appeared to influence the work reported in this paper.

Data Availability

Data will be made available on request.

Acknowledgement

We thank Dr. Coinneach Mackenzie Dover for the preparation of the perfluorodecyltrichlorosilane (FDTS) surfaces used in the experiments.

References

[1] J. Broadhead, S.K.E. Rouan, C.T. Rhodes, The spray drying of pharmaceuticals, Drug Dev. Ind. Pharm. 18 (1992) 1169–1206.
[2] B.-J. de Gans, P.C. Duineveld, U.S. Schubert, Inkjet printing of polymers: state of the art and future developments, Adv. Mater. 16 (2004) 203–213.
[3] Drying Technologies in Food Processing. Chen, X.D. , Mujumdar, A.S., Eds; John Wiley & Sons, 2009.
[4] L. Chen, J.R. Evans, Drying of colloidal droplets on superhydrophobic surfaces, J. Colloid Interface Sci. 351 (1) (2010) 283–287.
[5] P. Lebedev-Stepanov, S. Efimov, A. Kobelev, Drying droplet deposited on poor wetting substrate: beyond the lubrication approximation, Journal of Physics: Conference Series 925 (1) (2017), 012004.
[6] C.N. Kaplan, L. Mahadevan, Evaporation-driven ring and film deposition from colloidal droplets, J. Fluid Mech. (2015) 781.
[7] F. Du, L. Zhang, W. Shen, Controllable dried patterns of colloidal drops, J. Colloid Interface Sci. 606 (2022) 758–767.
[8] M. Parsa, S. Harmand, K. Sefiane, Mechanisms of pattern formation from dried sessile drops, Adv. Colloid Interface Sci. 254 (2018) 22–47.
[9] M. Härth, D.W. Schubert, Simple approach for spreading dynamics of polymeric fluids, Macromol. Chem. Phys. 213 (6) (2012) 654–665.
[10] L. Bansal, P. Seth, B. Murugappan, S. Basu, Suppression of coffee ring:(Particle) size matters, Appl. Phys. Lett. 112 (21) (2018), 211605.
[11] T.K. Pradhan, P.K. Panigrahi, Suppressing internal convection of a droplet using confinement during protein crystallization, J. Appl. Phys. 128 (8) (2020), 084701.
[12] M.J. Hertaeg, R.F. Tabor, G. Garnier, Effect of protein adsorption on the radial wicking of blood droplets in paper, J. Colloid Interface Sci. 528 (2018) 116–123.
[13] B. Pathak, S. Basu, Phenomenology and control of buckling dynamics in multicomponent colloidal droplets, J. Appl. Phys. 117 (24) (2015), 244901.
[14] R.D. Deegan, O. Bakajin, T.F. Dupont, G. Huber, S.R. Nagel, T.A. Witten, Capillary flow as the cause of ring stains from dried liquid drops, Nature 389 (1997) 827.
[15] B.M. Weon, J.H. Je, Self-pinning by colloids confined at a contact line, Phys. Rev. Lett. 110 (2) (2013), 028303.
[16] R.G. Picknett, R. Bexon, The evaporation of sessile or pendant drops in still air, J. Colloid Interface Sci. 61 (1977) 336–350.
[17] H. Hu, R.G. Larson, Evaporation of a sessile droplet on a substrate, J. Phys. Chem. B 106 (2002) 1334–1344.
[18] K.L. Maki, S. Kumar, Fast evaporation of spreading droplets of colloidal suspensions, Langmuir 18 (2011) 11347–11363.
[19] P.J. Yunker, T. Still, M.A. Lohr, A.G. Yodh, Suppression of the coffee-ring effect by shape-dependent capillary interactions, Nature 476 (2011) 308–311.
[20] N.D. Patil, R. Bhardwaj, A. Sharma, Self-sorting of bidispersed colloidal particles near contact line of an evaporating sessile droplet, Langmuir 34 (40) (2018) 12058–12070.
[21] T. Pham, S. Kumar, Drying of droplets of colloidal suspensions on rough substrates, Langmuir 33 (2017) 10061–10076.
[22] N. Tsapis, E.R. Dufresne, S.S. Sinha, C.S. Riera, J.W. Hutchinson, L. Mahadevan, D. A. Weitz, Onset of buckling in drying droplets of colloidal suspensions, Phys. Rev. Lett. 94 (1) (2005), 018302.
[23] G. Finotello, R.F. Kooiman, J.T. Padding, K.A. Buist, A. Jongsma, F. Innings, J.A. M. Kuipers, The dynamics of milk droplet–droplet collisions, Exp. Fluids 59 (1) (2018) 1–19.
[24] C. Sadek, P. Schuck, Y. Fallourd, N. Pradeau, R. Jeantet, C. Le Floch-Fouere, Buckling and collapse during drying of a single aqueous dispersion of casein micelle droplet, Food Hydrocoll. 52 (2016) 161–166.
[25] N. Fu, M.W. Woo, C. Selomulya, X.D. Chen, Shrinkage behaviour of skim milk droplets during air drying, J. Food Eng. 116 (1) (2013) 37–44.
[26] V. Kubyshkina, K. Sefiane, D. Orejon, C.M. Dover, Droplet interplay on microdecorated substrates, in: Advances in Heat Transfer and Thermal Engineering, Springer, Singapore, 2021, pp. 79–82.
[27] R. Tekidou, G. Duursma, C. Mackenzie-Dover, V. Kubyshkina, J. Terry, K. Sefiane, Wetting phenomena observed in evaporating droplets on structured surfaces, Heat Transf. Eng. 41 (19–20) (2020) 1645–1653.
[28] P. Lebedev-Stepanov, K. Vlasov, Simulation of self-assembly in an evaporating droplet of colloidal solution by dissipative particle dynamics, Colloids Surf. A: Physicochem. Eng. Asp. 432 (2013) 132–138.
[29] L. Pauchard, C. Allain, Buckling instability induced by polymer solution drying, EPL (Europhys. Lett.) 62 (6) (2003) 897.
[30] T. Yakhno, Salt-induced protein phase transitions in drying drops, J. Colloid Interface Sci. 318 (2) (2008) 225–230.
[31] G. Chen, G.J. Mohamed, Complex protein patterns formation via salt-induced self-assembly and droplet evaporation, Eur. Phys. J. E 33 (1) (2010) 19–26.
[32] D. Brutin, B. Sobac, B. Loquet, J. Sampol, Pattern formation in drying drops of blood, J. Fluid Mech. 667 (2011) 85–95.
[33] M.D. Choudhury, T. Dutta, S. Tarafdar, Pattern formation in droplets of starch gels containing NaCl dried on different surfaces, Colloids Surf. A 432 (2013) 110–118.